Multi-scale modelling of the blood chamber of a left ventricular assist device

Magdalena Kopernik[*] and Andrzej Milenin

AGH University of Science and Technology, Kraków, Poland

Abstract. This paper examines the blood chamber of a left ventricular assist device (LVAD) under static loading conditions and standard operating temperatures. The LVAD's walls are made of a temperature-sensitive polymer (ChronoFlex C 55D) and are covered with a titanium nitride (TiN) nano-coating (deposited by laser ablation) to improve their haemocompatibility. A loss of cohesion may be observed near the coating-substrate boundary. Therefore, a micro-scale stress-strain analysis of the multilayered blood chamber was conducted with FE (finite element) code. The multi-scale model included a macro-model of the LVAD's blood chamber and a micro-model of the TiN coating. The theories of non-linear elasticity and elasto-plasticity were applied. The formulated problems were solved with a finite element method. The micro-scale problem was solved for a representative volume element (RVE). This micro-model accounted for the residual stress, a material model of the TiN coating, the stress results under loading pressures, the thickness of the TiN coating and the wave parameters of the TiN surface. The numerical results (displacements and strains) were experimentally validated using digital image correlation (DIC) during static blood pressure deformations. The maximum strain and stress were determined at static pressure steps in a macro-scale FE simulation. The strain and stress were also computed at the same loading conditions in a micro-scale FE simulation.

Keywords: finite element method (FEM); representative volume element (RVE); polymer; nano-coating; titanium nitride (TiN); digital image correlation (DIC); left ventricular assist device (LVAD)

1. Introduction

The pneumatic Polish left ventricular assist device (POLVAD_EXT; Sarna *et al.* 2010) is composed of a blood chamber and two connectors (Fig. 1). The assembled device is 157 mm in length, 56 mm in width and 51 mm in height. The basic hydrodynamic parameters of POLVAD_EXT are as follows: an average flow of 2-5 dm^3/min, a ventricular stroke volume of 80-90 cm^3, a typical loading pressure of 90-160 mmHg in the outlet connector and 15 mmHg in the inlet connector and a pressure rise of less than 4700 mmHg/s. The LVAD's walls are made of an elastic, temperature-sensitive polymer (ChronoFlex C 55D) and are covered with an elastic-plastic titanium nitride (TiN) nano-coating, deposited by laser ablation, to improve their haemocompatibility (Ebner *et al.* 2006). The blood chamber has a layered structure. Fractures may

---

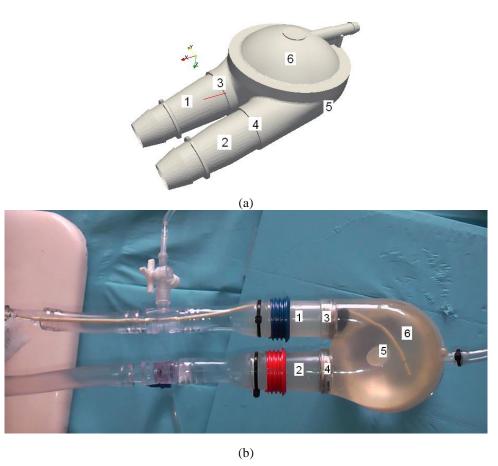*Corresponding author, Ph.D., E-mail: kopernik@agh.edu.pl

(a)

(b)

Fig. 1 (a) A CAD model and (b) a physical model of POLVAD_EXT. 1 and 2 – connectors; 3 and 4 – valves; 5 – blood chamber; 6 – pneumatic chamber with membrane (not clearly visible in the selected photo)

be observed next to the coating-substrate boundary. Therefore, a detailed stress-strain analysis is needed at the micro- and macro-scales.

Similar pneumatic and polymeric ventricular assist devices include the following models (Gregory *et al.* 2011): Abiomed AB5000 (USA), Thoratec PVAD (USA), Berlin Heart EXCOR (Germany) and Medos HIA-VAD (Germany). None of the aforementioned VADs is coated. The construction of the proposed Polish LVAD is closest to the Medos device. Most of the published works on VAD problems focus on numerical research. However, this type of analysis only leads to blood flow characteristics at the macro- (Fraser *et al.* 2011) and micro-scales (Pan *et al.* 2011, Yamaguchi *et al.* 2010). In summary, no physical or numerical models of multilayer LVADs are available in the literature. The proposed LVAD has a unique construction. Thus, the authors' work can be considered state of art.

In their previous work, the authors solved the micro- and macro-scale linear elasticity problems with a FE computer program. A macro-scale model of the blood chamber and a micro-scale model of the TiN (deposited on the polymer) were developed. In the first step, a comparative analysis of the latest POLVAD_EXT construction and its prior version (POLVAD) was performed (Milenin and Kopernik 2011a). Numerical comparison of the LVADs suggested that the newer blood

chamber generated less stress and strain, resulting in a smaller probability of fracture near the coating-substrate boundary than its predecessor. Therefore, POLVAD_EXT seems to have a better construction than POLVAD. However, the strain values were only obtained in the linear elastic zones of the LVADs. In the second step, a material model of the TiN coating and its residual stresses was constructed (Kopernik *et al.* 2011). This model enabled the development of an advanced micro-model that accounts for the following: the residual stress, material models of the substrate and the TiN coating, stress results from the macro-model under loading, TiN thickness and the wave parameters of the TiN surface (wavelength and amplitude). An extended version of the micro-model was investigated (Milenin and Kopernik 2011b) by applying factor analysis to both LVADs (POLVAD and POLVAD_EXT). There was no difference between the maximum stress and strain localisations in POLVAD and POLVAD_EXT. However, the POLVAD_EXT micro-model had smaller stresses and strains than POLVAD.

The novel goals of the present work are as follows:

(a) Application of a static set of loads at two critical pressure values (37.3 kPa and -10 kPa) and an operating temperature of 37 ℃ in macro- and micro-models of POLVAD_EXT;

(b) Macro-scale validation of the non-linear FE solution with digital image correlation (DIC) data (displacements and strains) from the blood chamber's external surface.

2. Materials and methods

2.1 Experiments

The proposed multi-scale model (POLVAD_EXT) required experimental verification and input data. The following experiments were performed at the Foundation of Cardiac Surgery Development in Zabrze, Poland, to provide additional data for this macro-model:

(a) A static, uniaxial tension test was conducted on 12 specimens of the ChronoFlex C 55D polymer at two temperatures (21℃ and 38℃). The polymer was stretched with a velocity of 10 mm/min. The dimensions of the specimens were 4.09±0.04 mm thick, 6.11±0.07 mm wide and 35 mm long. The specimens were prepared by an injection method and were tested on a MTS Criterion Single machine that was equipped with a 5 kN force sensor. The registered data were analysed in MTS TestWorks™ software. Tests and calculations were performed according to the ISO 527-2 and ASTM D 638 standards. A material model of the polymer is represented by Eq. (1)

$$\sigma_i = 104.54\varepsilon_i^{0.75}\exp(-3.37\varepsilon_i)\exp(-0.04t) \tag{1}$$

where: t – temperature, ε_i – effective strain, σ_i – effective stress. This non-linear, elastic model (Eq. (1)) was used as input data in the POLVAD_EXT macro-model.

(b) Digital image correlation (Orteu 2009) was used to analyse fields of deformation on the external surface of the POLVAD_EXT's blood chamber. These experiments were conducted under a static set of pressures (ranging from 37.3 kPa to -10 kPa) and at an operating temperature of 37 ℃. The static pressure applied in these experiments (37.3 kPa) was critical; its value was inflated compared to physiological conditions. Testing medical devices in overestimated conditions is typical and recommended. For example, the maximum pressure in the cardiac cycle is 120 mmHg (16 kPa), whereas it was 280 mmHg (37.3 kPa) in the experiment. The following components were used in the experiment (Fig. 2): a Q-400 head (Dantec Dynamics GmbH, Ulm,

Fig. 2 An overview of the DIC experimental setup: 1 – PC and electronic system, 2 – tank and temperature stabilising system, 3 – centrifugal pump, 4 – pneumatic pump, and 5 – cameras

Germany) that contained two CCD cameras in a stereoscopic system, light sources (LED) and ISTRA 4D software (installed on a laptop). The examined POLVAD_EXT device was connected to drains that were attached to a heated water bath. A constant water flow (0.1 l/min) was maintained by a centrifugal pump. Images were taken after stabilisation at specified pressures (-3.3, -6 and -10 kPa or 11, 16, 24, 29 and 37.3 kPa). A sample image is presented in Fig. 3(a). The POLVAD_EXT boundary conditions (Fig. 3(b)) in the FE model were based on the DIC settings. Therefore, the displacements and strains recorded in the DIC tests could be compared to the computational results of the FE macro-model.

The following experiments were previously conducted by the authors (Kopernik *at al*. 2011) to supplement the data for this micro-model:

(a) A nano-indentation test and an inverse analysis were used to determine the mechanical properties of the TiN coating. The parameters of the TiN coating's bilinear, elastic-plastic material model were identified as follows: $\varepsilon_1 = 0.009$, $\sigma_1 = 2\ 614$ MPa, $\varepsilon_2 = 0.166$ and $\sigma_2 = 9\ 107$ MPa.

(b) The compressive residual stress of the TiN coating was 2 GPa based on TEM (Transmission Electron Microscopy) images.

(c) The TiN coating's sinusoidal shape was observed in the TEM images (Fig. 4). According to the experimental studies, the TiN coating's wave characteristics were as follows: a thickness of 350 nm, an amplitude of 50 nm and a wavelength of 350 nm.

2.2 Model

A two-scale model was considered: a macro-model of the POLVAD_EXT's blood chamber and a micro-model of the TiN nano-coating. The micro-scale problem was solved for a representative volume element (RVE). The parameters corresponding to the macro-scale model (the macro-parameters) were denoted by a superscript *M,* such as the macro-stress σ^M. The RVE's micro-scale parameters (the micro-parameters) were denoted by a superscript *m*, such as the micro-stress σ^m. The average values of the RVE variables were denoted by an upper bar, for

pressure   free surface   fixed surface
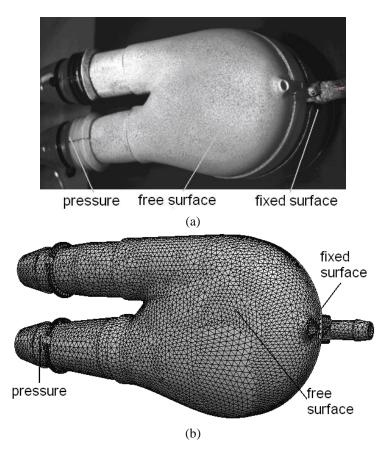
(a)

fixed surface

pressure

free surface

(b)

Fig. 3 POLVAD_EXT diagrams for the DIC model: (a) The DIC settings are marked on an image of the physical model as captured by one of the cameras and (b) the boundary conditions of the FE model
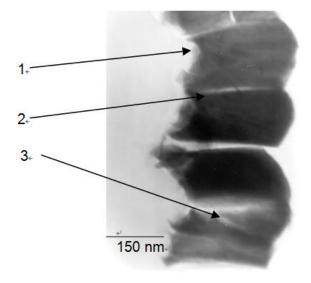

1

2

3

150 nm

Fig. 4 An overview of the DIC experimental setup: 1 – PC and electronic system, 2 – tank and temperature stabilising system, 3 – centrifugal pump, 4 – pneumatic pump, and 5 – cameras

example, the mean micro-stress $\bar{\sigma}^m$. In the two-scale model, the macro-stress σ_{ij}^M and the macro-strain ε_{ij}^M tensors corresponding to point X^M in the macro-model were directly evaluated by the average volume of the micro-stress σ_{ij}^m and the micro-strain ε_{ij}^m in the RVE.

2.2.1 Macro-model

The POLVAD_EXT model was prepared using the authors' FE code. Within the code, the non-linear elastic and elastic-plastic FE problems were solved in the macro- and micro-scales under static loadings (pressure and underpressure) and at the blood chamber's operating temperature. The FE macro-model indicated the failure source areas in the loaded construction based on strain-stress analysis.

The macro-scale boundary problem was formulated using the theory of non-linear elasticity and the distribution of displacements U_i^M. The proposed approach described the deformation of the POLVAD_EXT chamber under blood pressure when its stresses were related to strains by nonlinear equations (according to the nonlinear theory of elasticity) and when the strain disappeared in non-loading conditions. The non-linearity in the elastic deformation process of the blood chamber was the result of the non-linear mechanical properties of the ChronoFlex C 55D polymer and the TiN coating.

The macro-scale blood chamber deformation problem required a 3D solution. Thus, the boundary problem was defined by the theory of non-linear elasticity and was composed of groups of equations, as described in (Milenin 2010). In the non-linear zone of deformation, the effective stress σ_i^M was a function of the effective strain ε_i^M and the temperature t. Each iteration used the effective modulus instead of the Young's modulus. The convergence problems associated with the macro-scale model's nonlinearities were solved by an iterative method. The effective Young's modulus E_{eff} was calculated in the next iteration $k+1$ by Eq. (2)

$$E_{eff}^{M(k+1)} = \frac{\sigma_i^{M(k)}}{\varepsilon_i^{M(k)}} \tag{2}$$

where: $E_{eff}^{M(k+1)}$ - effective Young's modulus in the next iteration, $\sigma_i^{M(k)}$ and $\varepsilon_i^{M(k)}$ - effective stress and effective strain in current iteration, respectively, k – number of iterations.

The error of the effective Young's modulus δ was calculated by Eq. (3)

$$\delta = \frac{E_{eff}^{M(k)} - E_{eff}^{M(k+1)}}{E_{eff}^{M(k)}} \tag{3}$$

where: $E_{eff}^{M(k)}$ – effective Young's modulus in the previous iteration, $E_{eff}^{M(k+1)}$ – value calculated in Eq. (2).

The relation $\sigma_i^M\left(\varepsilon_i^M, t\right)$ was determined according to Eq. (1). The components of stiffness matrix $[K]$ and the complete load vector $\{F\}$ were established according to Eqs. (4) and (5)

$$[K_e^M] = \int_{V_e} [B]^T [D^M][B]dV \tag{4}$$

$$\{F_e^M\} = -\int_{S_e} [N]^T \{P^M\}dS \tag{5}$$

where: S – contact surface, $\{P^M\}$ – pressure inside the blood chamber, $[B]$ – matrix containing derivatives of the shape functions, $[D^M]$ – matrix containing appropriate material properties (E^M, v^M), $[N]$ – matrix of the shape functions in the finite element, V – volume, V_e – volume of the current finite element e, S_e – contact surface between the current element and the blood chamber.

A tetrahedron element with a five–point integration scheme was used in the POLVAD_EXT macro-model. The average number of applied nodes was 50,000, and the average number of applied tetrahedron elements was 150,000. The boundary conditions of the blood chamber were set according to the DIC settings (Fig. 3) and were as follows: (a) the distribution of blood pressure was $P^M = P$ (critical pressures are 37.3 kPa and -10 kPa) on the inner surface of the blood chamber, (b) there were fixed surfaces on the outer, upper part (no displacement in the Z direction) and (c) there were non-fixed surfaces on the outer part (no loading).

2.2.2 Micro-model

The results of the strain analysis on the inner surface of the POLV_EXT's blood chamber (acquired from the macro-scale FE model) were used to find the areas with the greatest tendency for failure. The FE elements with the maximum strain and stress values were located between the two connectors on the inner surface of the blood chamber. These results were further examined in the micro-scale model. The micro-scale model of the TiN/polymer layers was enriched with surface irregularities (roughness) due to the TiN nano-coating. The coating was represented by a periodic function (Wiklund *et al.* 1999) with three key parameters: amplitude, wavelength and thickness. The micro-model incorporated the following experimental parameters (see section 2.1): residual stress, shape parameters of the coating surface's wave characteristics and material models of the TiN coating and the polymer. The representative volume element was composed of the polymer and the TiN nano-coating. The non-linearity of the mechanical properties between the TiN coating and the polymer was observed. Thus, an elastic-plastic and a non-linear elastic material model, as well as their corresponding theories, are used in the computations.

The micro-scale boundary problem, which included the unloading process, was solved by the FE micro-model. The initial stress $\{\sigma_{0res}\}$ in the TiN nano-coating was applied in the FE formulation. The relationship between the stresses and strains was established using a matrix (vector) definition

$$\{\sigma^m\} = [D^m]\{\varepsilon^m\} - \{\sigma^m_{0res}\} \tag{6}$$

where: $\{\sigma^m_{0res}\}$ – residual stress; $\{\sigma^m\}$ and $\{\varepsilon^m\}$ – stress and strain tensors in vector format.

The variational principle of the non-linear elastic and elastic-plastic theories led to the following functional form for the finite element e in the RVE

$$W = \int_{V_e} \frac{1}{2}\{U^m\}^T [B]^T [D^m][B]\{U^m\}dV - \int_{V_e} \{U^m\}^T [B]^T \{\overline{\sigma}^m_{0res}\}dV - \int_{S_e} \{U^m\}^T [\overline{N}]^T \{p^m\}dS \tag{7}$$

where: $\{U^m\}$ – nodal displacement vector in the elements; $\overline{\sigma}^m_{0res}$ – experimental value of the residual stress in the current finite element e.

The effective Young's modulus (Eq. (2)) was used in the elastic zone (instead of the Young's modulus) to linearise the function in Eq. (7) for a non-linear problem

$$E_{eff}^m = \frac{\sigma_i^m}{\varepsilon_i^m} \tag{8}$$

The stiffness matrix $[K]$ (Eq. (4)) and the load vector $\{F\}$ (Eq. (5)) were established in the following forms

$$[K_e^m] = \int_{V_e} [B]^T [D^m][B]dV \tag{9}$$

$$\{F_e^m\} = -\int_{V_e} \{U^m\}^T [B]^T \{\overline{\sigma}_{0res}^m\}dV - \int_S [\overline{N}]^T \{p^m\}dS \tag{10}$$

The residual stress in the TiN nano-coating was evaluated before the loading simulations. After implementation of the residual stress $\overline{\sigma}_{0\,res}$, the micro-scale simulations of loading and unloading were performed.

The periodic boundary conditions (PBC) were used in parallel to the direction of the blood chamber's surface, while the static boundary conditions were applied in the direction of the blood pressure. The following modification of the PBC was proposed to account for the TiN nano-coating. The deformation tensor was taken from the macro-scale model of the boundary conditions for the RVE. The direction normal to the surface of the RVE corresponded to the direction of the hydrostatic pressure p (blood pressure p^m) on the TiN nano-coating. Therefore, shear stresses and strains were not present on this surface, and p was a principal stress in the stress tensor. Thus, the solution in main coordinate system was found. The principal strains were used as boundary conditions in the RVE. Each side of the RVE was a symmetric plane with respect to these boundary conditions; their shear stresses and strains were all zero.

Four–node finite elements were used. A strain ε_2^M (second principal strain of the strain tensor) was introduced as a constant in the micro-scale model. Therefore, the 3D boundary problem of the RVE deformation was transformed to 2D plane strain problem with a prescribed value of the strain ε_2^M. The principal strain ε_1^M and the pressure $p^M = p^m = p$ were also used in the RVE model.

3. Results and discussion

The POLVAD_EXT macro-model was developed using the experimental data specified in section 2.1 and the model description shown in subsection 2.2.1.

Simulations of the POLVAD_EXT's blood chamber (made of ChronoFlex C 55D) were performed at a temperature of 37 ℃ and under loading at two critical pressures, -10 kPa and 37.3 kPa. The Z-directional displacements, which were obtained on the external surface of the macro-model by the authors' FE code, were compared with the DIC results (Figs. 5 and 6).

According to the DIC experiment, the maximum Z-directional displacement (1.4 mm) was observed on the external surface of the blood chamber at a pressure of 37.3 kPa (Fig. 5(a)).

A similar result (1.3 mm) was computed by the FE macro-model of the blood chamber (Fig. 5(b)). At a pressure of -10 kPa, the maximum experimental Z-directional displacement was -0.3 mm (Fig. 6(a)), and the maximum numerical displacement was -0.25 mm (Fig. 6(b)).

A comparison of the experimental and numerical displacements at a central point on the
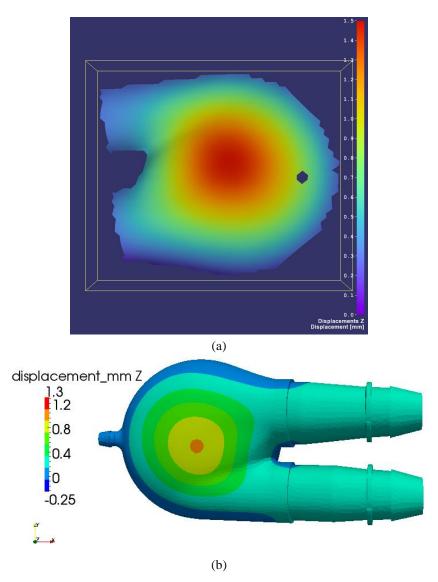
(a)

(b)

Fig. 5 The *Z*-directional displacement distribution on the external surface of the POLVAD_EXT blood
    chamber at a pressure of 37.3 kPa: (a) The DIC values (in mm) and (b) the FE model's values (in mm)

external surface of blood chamber indicated a good quantitative agreement between the results
at both pressures. The *Z*-directional displacement distributions were regular and similar in the
simulation and the experiment. Therefore, it was concluded that the numerical and experimental
results also have good qualitative agreement.

The *X*-directional principal strains on the external surface of macro-model (obtained by the
authors' FE code) were compared with the DIC results (Figs. 7 and 8). At a pressure of 37.3 kPa,
the maximum *X*-directional strain was the same (0.012) in the DIC experiment (Fig. 7(a)) and in
the FE macro-model (Fig. 7(b)). At a pressure of -10 kPa, the maximum experimentally measured
X-directional strain was 0.005 (Fig. 8(a)), whereas the maximum computed *X*-directional strain
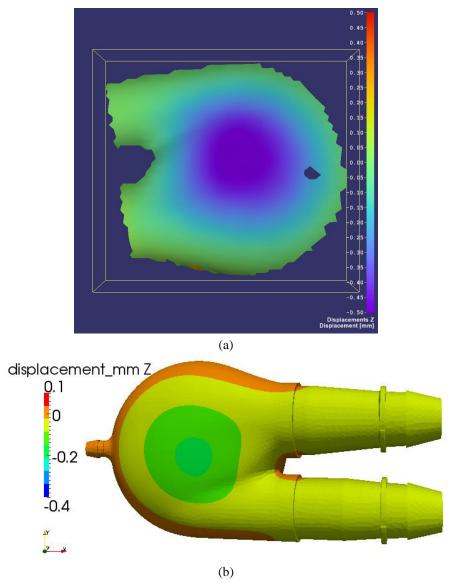
(a)

(b)

Fig. 6 The distribution of *Z*-directional displacements on the external surface of the POLVAD_EXT blood
chamber at a pressure of -10 kPa: (a) The DIC values (in mm) and (b) the FE model's values (in mm)

was 0.002 (Fig. 8(b)). A comparison of the experimental and numerical data on the *X*-directional principal strains for a central point on the blood chamber's external surface indicated a good quantitative agreement between the results at 37.3 kPa. The qualitative agreement between the numerical and experimental strains was poor due to the non-regular distributions of the experimental strains, especially at -10 kPa.

Analysis of the results revealed that there were errors in the obtained data. The error sources were distinguished as follows:
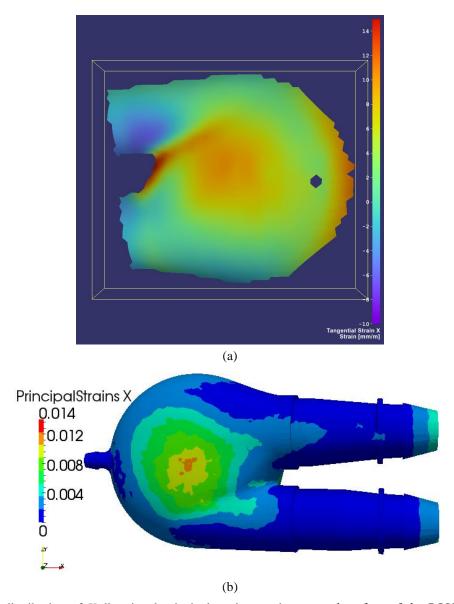
(a)

(b)

Fig. 7 The distribution of *X*-directional principal strains on the external surface of the POLVAD_EXT's blood chamber at a pressure of 37.3 kPa: (a) The DIC results (the numerical values x 10^{-3}) and (b) the FE model's results

(a) Measurement errors in the DIC experiment. The roughness on the surface of the blood chamber was due to hand application of the paint. The paint on the blood chamber surface was not perfectly regular; it dried and, after a certain period of time, it fell off. The surface of blood chamber was not flat; it contained curves and irregularities that could be viewed in the camera images. It was not possible to track the exact same point location on such an irregular surface. The blood chamber was permanently fixed in the experiment, but it was difficult to completely
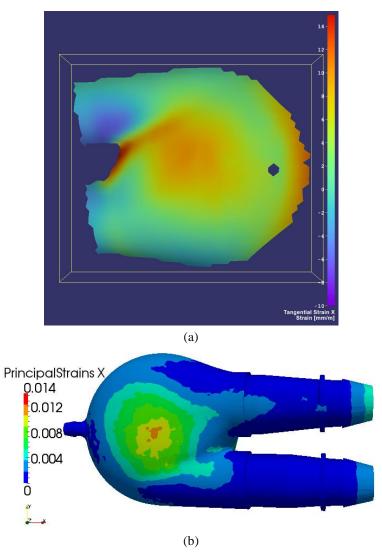
(a)

(b)

Fig. 8 The distribution of X-directional principal strains on the external surface of the POLVAD_EXT's blood chamber at a pressure of -10 kPa: (a) The DIC results (the numerical values x 10^{-3}) and (b) the FE model's results

eliminate its movements during the experiment. These movements were especially visible in the small strain distributions that were measured by DIC at -10 kPa, as they had larger strain distribution irregularities at this value.

(b) The blood chamber material was temperature sensitive. The blood chamber could not be heated to a uniform temperature (37 °C) using a hydraulic water system. Furthermore, a homogenous temperature distribution could not be obtained on the blood chamber's external surface because the device was still in contact with environment (20-25 °C are typical environmental temperatures for working LVADs). The blood chamber could not be perfectly deformed in all directions by applying pressure on its internal surface. Consequently, a uniform
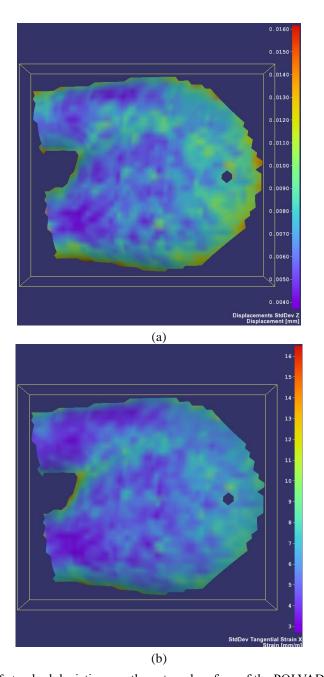
(a)

(b)

Fig. 9 The distribution of standard deviations on the external surface of the POLVAD_EXT's blood chamber at a pressure of 37.3 kPa as computed for (a) the *Z*-directional displacement (in mm) and (b) the X-directional principal strains (numerical values x 10^{-3})

strain distribution could not be obtained on the external surface.

(c) The FE model of the blood chamber required the solution of a non-linear elastic problem. This solution introduced a computational error that is typical for non-linear tasks.
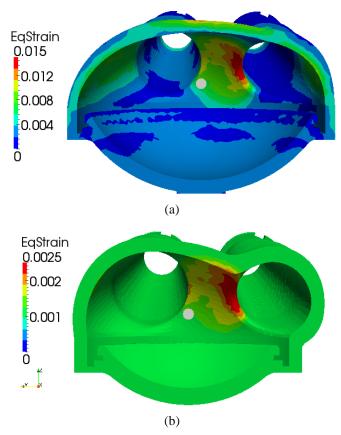
(a)

(b)

Fig. 10 The effective strain distribution on the internal surface of the POLVAD_EXT's blood chamber, as calculated by the FE model at pressures of (a) 37.3 kPa and (b) -10 kPa. The grey points that are visible are the results of a visualisation tool; they do not have any numerical meaning

(d) The CAD model of the LVAD was not exactly the same as the physical model; there were several small differences in their dimensions.

The standard deviation of the displacements was less than 2%, as computed by the DIC software. The standard deviation of the strains was less than 20%. The smaller strains had greater displacements at the lower pressure value (-10 kPa). The typical and representative error distributions (standard deviation) are shown in Fig. 9 for the errors in the *Z*-directional displacements and the *X*-directional principal strains at a pressure of 37.3 kPa.

A strain-stress state was reached by applying a load in the POLVAD_EXT macro-model. Afterwards, the micro-model was used to compute the maximum of the function *f* in the FE elements according to Eq. (11):

$$f = \varepsilon_i k = \varepsilon_i \frac{\sigma_0}{\sigma_i} \qquad (11)$$

where: k – triaxiality factor, ε_i – effective strain, σ_0 – mean stress, σ_i – effective stress.

The function *f* was calculated for the largest values of the effective strain (0.015 in Fig. 10(a)) and stress (1000 kPa in Fig. 11(a)), which were identified on the inner surface of the VAD
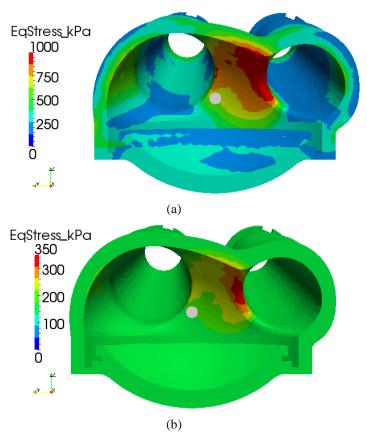
(a)

(b)

Fig. 11 The effective stress distribution on the internal surface of the POLVAD_EXT's blood chamber, as calculated by the FE model at pressures of (a) 37.3 kPa and (b) -10 kPa. The grey points that are visible are the results of a visualisation tool; they do not have any numerical meaning

between its two connectors at a pressure of 37.3 kPa. The same region of the inner surface was further analysed in the macro-model at a pressure of -10 kPa. The strain was 0.025 in Fig. 10(b), and the stress was 350 kPa in Fig. 11(b). The maximum values of principal strains in specified regions of the blood chamber's internal surface were introduced into the micro-model. These values were as follows:

- $\varepsilon_1 = 0.0133$, $\varepsilon_2 = -0.00163$, $p = 37.3$ kPa and

- $\varepsilon_1 = 0.002475$, $\varepsilon_2 = -0.000323$, $p = -10$ kPa

The micro-model of the TiN/polymer was developed using the experimental data specified in section 2.1 and the model description shown in subsection 2.2.2.

The specimen analysed in the micro-model simulation had a thickness of 1850 nm and a width of 6000 nm. The thickness selection of the TiN coating was critical. At its largest, the deposited thickness was 350 nm. This coating thickness was used in the simulations.

Experimental studies have shown that the thickness of the coating often leads to facture. This
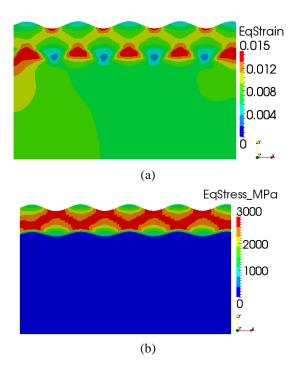
(a)

(b)

Fig. 12 The local distributions of (a) the effective strain and (b) the effective stress computed at a pressure of 37.3 kPa
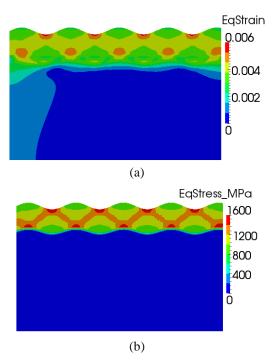

(a)

(b)

Fig. 13 The local distributions of (a) the effective strain and (b) the effective stress computed at a pressure of -10 kPa

observation was also noted in the present paper. Loading simulations of the micro-model were performed at pressures of 37.3 kPa (Fig. 12) and -10 kPa (Fig. 13) and at a temperature of 37 ℃. The polymer's maximum effective strain and stress were located near the coating-polymer boundary. The maximum values of the selected parameters were as follows:

· At a pressure of 37.3 kPa, the effective strain was 0.015, and the effective stress was 3000 MPa.
· At a pressure of -10 kPa, the effective strain was 0.006, and the effective stress was 1600 MPa.

It should be noted that the computed strain and stress values were larger at the overestimated pressure (37.3 kPa) than at -10 kPa. This result simulated the effects of critical conditions. Thus, because a danger zone (i.e. an area of maximum stress and strain) was identified near the coating-polymer boundary, further experimental and numerical investigations are needed to evaluate the material's connection quality over long-term use.

All of the computed micro-parameters displayed large differences between the two pressures. The effective strain and stress were almost twice as large at the higher pressure (37.3 kPa) than at the lower pressure (-10 kPa). The maximum values of the effective strain were in the elastic range of the blood chamber materials at loading pressures of -10 kPa and 37.3 kPa. Therefore, the micro-model of the walls of POLVAD_EXT was reversibly deformed.

The residual stress and the mechanical properties of the nano-coating (a material model of the TiN coating) could not be adequately estimated due to the limited number of experiments. Thus, the micro-model's results should be considered more qualitatively than quantitatively at this stage. However, the macro-model's results are more reliable due to experimental validation (DIC), as well as the correctness and repeatability of the input data (the tension tests of the polymer).

4. Conclusions

(1) A comparison of the experimental (DIC) and the numerical (FEM) results on the external surface of the POLVAD_EXT's blood chamber showed acceptable levels of quantitative and qualitative agreement, especially for the displacement distributions at a pressure of 37.3 kPa. However, the results were not error free.

(2) The maximum effective strain and the maximum effective stress on the inner surface of POLVAD_EXT macro-model were identified in the area between the two connectors.

(3) The maximum values of the effective strain and the effective stress were located in the polymer next to the coating-polymer boundary. While this location was not fractured in the models, it should be monitored, especially during long-term use of the blood chamber.

(4) The micro-model of the walls of the POLVAD_EXT was reversibly deformed.

Acknowledgements

References

Ebner, R., Lackner, J.M., Waldhauser, W., Major, R., Czarnowska, E., Kustosz, R., Lacki, P. and Major, B. (2006), "Biocompatibile TiN – based novel nanocrystalline films", *Bull. Pol. Ac. Tech.*, **54**, 167-173.

Fraser, K.H., Taskin, M.E., Griffith, B.P. and Wu, Z.J. (2011), "The use of computational fluid dynamics in the development of ventricular assist devices", *Med. Eng. Phys.*, **33**, 263-280.

Gregory, S.D., Timms, D., Gaddum, N., Mason, D.G. and Fraser, J.F. (2011), "Biventricular assist devices: a tchnical review", *Ann. Biomed. Eng.*, **39**, 2313-2328.

Kopernik, M., Milenin, A., Major, R. and Lackner, J.M. (2011), "Identification of material model of TiN using numerical simulation of nanoindentation test", *Mater. Sci. Tech.*, **27**, 604-616.

Milenin, A. (2010), *Bases of finite element method,* Akademia Górniczo-Hutnicza, Kraków. (in Polish)

Milenin, A. and Kopernik, M. (2011a), "Comparative analysis of ventricular assist devices POLVAD and POLVAD_EXT based on multiscale FEM model", *Acta Bioeng. Biomech.*, **13**(2), 13-23.

Milenin, A. and Kopernik, M. (2011b), "Microscale analysis of strain–stress state for TiN nanocoating of POLVAD and POLVAD_EXT", *Acta Bioeng. Biomech.*, **13**(4), 11-19.

Orteu, J.J. (2009), "3-D computer vision in experimental mechanics", *Opt. Laser Eng.*, **47**, 282-291.

Pan, W., Fedosov, D.A., Caswell, B. and Karniadakis, G.E. (2011), "Predicting dynamics and rheology of blood flow: a comparative study of multiscale and low-dimensional models of red blood cells", *Microvasc. Res.*, **82**, 163-170.

Sarna, J., Kustosz, R., Major, R., Lackner, J.M. and Major, B. (2010), "Polish artificial heart – new coatings, technology, diagnostics", *Bull. Pol. Ac. Tech.,* **58**, 329-335.

Wiklund, U., Gunnars, J. and Hogmark, S. (1999), "Influence of residual stresses on fracture and delamination of thin hard coatings", *Wear,* **232**, 262-269.

Yamaguchi, T., Ishikawa, T., Imai, Y., Matsuki, N., Xenos, M., Deng, Y. and Bluestein, D. (2010), "Particle-based methods for multiscale modeling of blood flow in the circulation and in devices: challenges and future directions", *Ann. Biomed. Eng.*, **38**, 1225-1235.

YY